# Understanding the Role of Ion Migration in the Operation of Perovskite Light Emitting Diodes by Transient Measurements

*Qi Dong[1], Juliana Mendes[1], Lei Lei[1], Dovletgeldi Seyitliyev[2], Liping Zhu[1], Siliang He[3], Kenan Gundogdu[2], Franky So[1*]*

*fso@ncsu.edu

[1]Department of Materials Science and Engineering, North Carolina State University, Raleigh, NC 27606, USA

[2]Department of Physics, North Carolina State University, Raleigh, NC 27607, USA

[3]Department of Chemical and Biomolecular Engineering, North Carolina State University, Raleigh, NC 27606, USA

**Key words**: ion migration, perovskite light-emitting diodes, transient electroluminescence, transient current, device physics, charge injection

**Abstract**

Perovskite light emitting diodes (LEDs) have been gaining attention in recent years due to the high efficiencies. Despite of the recent progress made in device efficiency, the operation mechanisms of these devices are still not well-understood, especially the effects of ion migration. In this work, the role of ion migration is investigated by measuring the transient electroluminescence and current responses, with both the current and efficiency showing a slow response in a time scale of tens of milliseconds. The results of the charge injection dynamics show that the slow response of the current is attributed to the migration and accumulation of halide ions at the anode interface, facilitating hole injection and leading to a strong charge imbalance. Further, the results of the charge recombination dynamics show that the slow response of the efficiency is attributed to enhanced charge injection facilitated by ion migration, which leads to an increased carrier density favoring bimolecular radiative recombination. Through a combined analysis of both charge injection and recombination dynamics, we finally present a comprehensive picture of the role of ion migration in device operation.

## 1. Introduction

Organometal halide perovskites have shown a great potential over the past decade for their applications of next-generation optoelectronic devices including photovoltaics,[1] transistors,[2] light-emitting diodes (LEDs)[3,4] and lasers[3,5] due to their unique properties of defect tolerance,[6–9] long carrier diffusion length,[10] high color purity,[11] bandgap tunability[12,13] and solution processability. Perovskite LEDs are specifically interesting because of the narrow emission bandwidth[11] compared with organic LEDs (OLEDs). To date, external quantum efficiencies (EQEs) above 20% have been achieved in both red[14,15] and green[16] perovskite LEDs. The rapid progress in device efficiency is mainly attributed to the structural and compositional engineering of perovskite light-emitting materials.[14–21] For example, high efficiency perovskite LEDs can be made by adding bulky organic cations in perovskites, not only promoting radiative recombination by forming low-dimensional nanostructures (quasi-2D perovskite[17–19] or nanocrystal perovskite[20]), but also suppressing non-radiative recombination through defect passivation.[21]

Despite the high efficiencies achieved by perovskite LEDs, an in-depth study of the role of ion migration on device operation is still lacking. Ion migration has been recognized as a key reason for photocurrent hysteresis in perovskite photovoltaics (PVs).[22–24] For perovskite light-emitting devices, ion migration leads to changes in the internal electric field affecting charge injection and electroluminescence (EL).[25–27] As a result, two interesting phenomena have been reported. The first phenomenon is polarity switchable EL which is done by applying an external bias in either direction to a device with two high work function electrodes.[25] Another phenomenon is reversible enhancement in charge injection and EL by pre-bias poling.[26,27] Both can be explained by enhanced charge injection as a result of ion accumulation at the electrode interfaces.[25–27] However, to further understand the role of ion migration in the operation of perovskite LEDs, three important issues

need to be addressed. First, since ion migration and hence the ion distribution is a dynamic process affected by the applied electric field, it will affect the results of device measurements during the luminescence-current-voltage (LIV) scans. Therefore, the EL intensity and current are strongly affected by the voltage scan rate as well as the scan direction, leading to an uncertainty in device measurements. Specifically, the apparent measured efficiency has been found to vary with the measurement parameters such as the scan rate, scan direction and pre-bias conditions.[20,27,28] Second, mobile ions accumulated at the electrode interface affect charge injection. Specifically, mobile cations affect hole injection and mobile anions affect electron injection.[25–27] Therefore, it is important to differentiate the effects of ion migration on electron and hole injection and their roles in the overall device performance. Third, in addition to charge injection, ion migration can also affect charge recombination through increased charge carrier density and defect annihilation,[29–31] which eventually contributes to the dynamics of EL. Therefore, to better understand the device operation mechanism, it is necessary to carry out transient EL and current measurements to monitor the dynamics of charge injection and recombination in perovskite LEDs and study the interplay of the effects on charge injection and recombination due to ion migration.

To synthesize perovskite nanocrystals for LED fabrication, we first passivate grain boundary defects and constrain the growth of perovskite crystals by adding a bulky organic cation phenethylammonium bromide (PEABr) to methylammonium lead bromide ($MAPbBr_3$). To study the device operation mechanism and the effects of ion migration on the device performance, transient electroluminescence (Tr-EL) and transient current (Tr-J) measurements were carried out, from which the transient efficiency (Tr-CE) data were also extracted. From the results, all three parameters show a very slow response in a time scale of tens of milliseconds. To have an in-depth understanding of the origin of the slow current response, Tr-J measurements on single carrier

devices were conducted to investigate the electron and hole injection dynamics separately and the results show that the slow response is due to a slow hole injection response as a result of migration and accumulation of Br ions at the anode interface facilitating hole injection. On the contrary, electron injection is not affected by Br ion migration. Such a different effect of ion migration on electron and hole injection leads to a strong charge imbalance in the resulting LEDs. To study the origin of the slow efficiency response, photoluminescence (PL) under pulse voltage measurements were conducted to investigate the charge recombination dynamics and the results show that the defect density is not reduced under an external electric field. Therefore, we attribute the increase of the efficiency to the enhanced charge injection facilitated by ion migration leading to an increased carrier density favoring bimolecular radiative recombination. Finally, a comprehensive picture of the device operation mechanisms will be presented.

## 2. Results and Discussions

### 2.1. Film Characterization and Device Characteristics

In this work, perovskite films were made by adding PEABr in $MAPbBr_3$ (in a molar ratio of 30%) to passivate grain boundary defects as well as to form low-dimensional perovskites for exciton confinement.[17–21] It is known that by adding bulky organic cations (PEABr in our case) to the perovskite precursors, either quasi-2D perovskite[17–19] or nanocrystal perovskite[20] can be formed. To determine the nanostructure of our perovskite films, UV-visible absorption and X-ray diffraction (XRD) measurements were conducted, and the results are shown in Figures 1 (a) and (b) respectively. From the UV-visible absorption spectrum, we do not observe any absorption peaks corresponding to 2D perovskites and the absorption band edge at 530 nm indicates that only 3D perovskite is present in our film. From the XRD pattern, again, we only observe a broad (100) diffraction peak of 3D perovskite at 14.8 degree, indicating the presence of perovskite nanocrystals.

Since the bulky organic cations do not contribute to the formation of quasi-2D perovskite, they function as an organic matrix in the presence of perovskite nanocrystals. Therefore, we conclude that our perovskite film consists of perovskite nanocrystals ($MAPbBr_3$) embedded in an organic matrix (PEABr).[20]

The perovskite LEDs used in our study have the following structure: ITO/ nickel oxide ($NiO_x$)/ perovskite (30% PEABr in $MAPbBr_3$)/ 2,2′,2"-(1,3,5-Benzinetriyl)-tris(1-phenyl-1-H-benzimidazole) (TPBi)/ $Cs_2CO_3$/ Al, where $NiO_x$ is used as hole transporting layer (HTL) and TPBi is used as electron transporting layer (ETL) (Figure 1 (c)). The device LIV characteristics are shown in Figure 1 (d), and a luminance above 2000 $cd/m^2$ is observed at 5 V. The device shows a maximum current efficiency of 22 cd/A corresponding to an EQE of 7.7% as shown in Figure 1 (e). The FWHM of the EL spectrum is 21 nm, indicating a good color purity (Figure 1 (f)). The peak wavelength of the EL spectrum is at 521 nm which is shorter than that of bulk $MAPbBr_3$ perovskite, corresponding to the reduced crystal size.[20] Here, the performance of the perovskite LED is comparable to those reported in the literature,[17–20] and therefore these devices can be used as a good reference to study ion migration in perovskite LEDs.

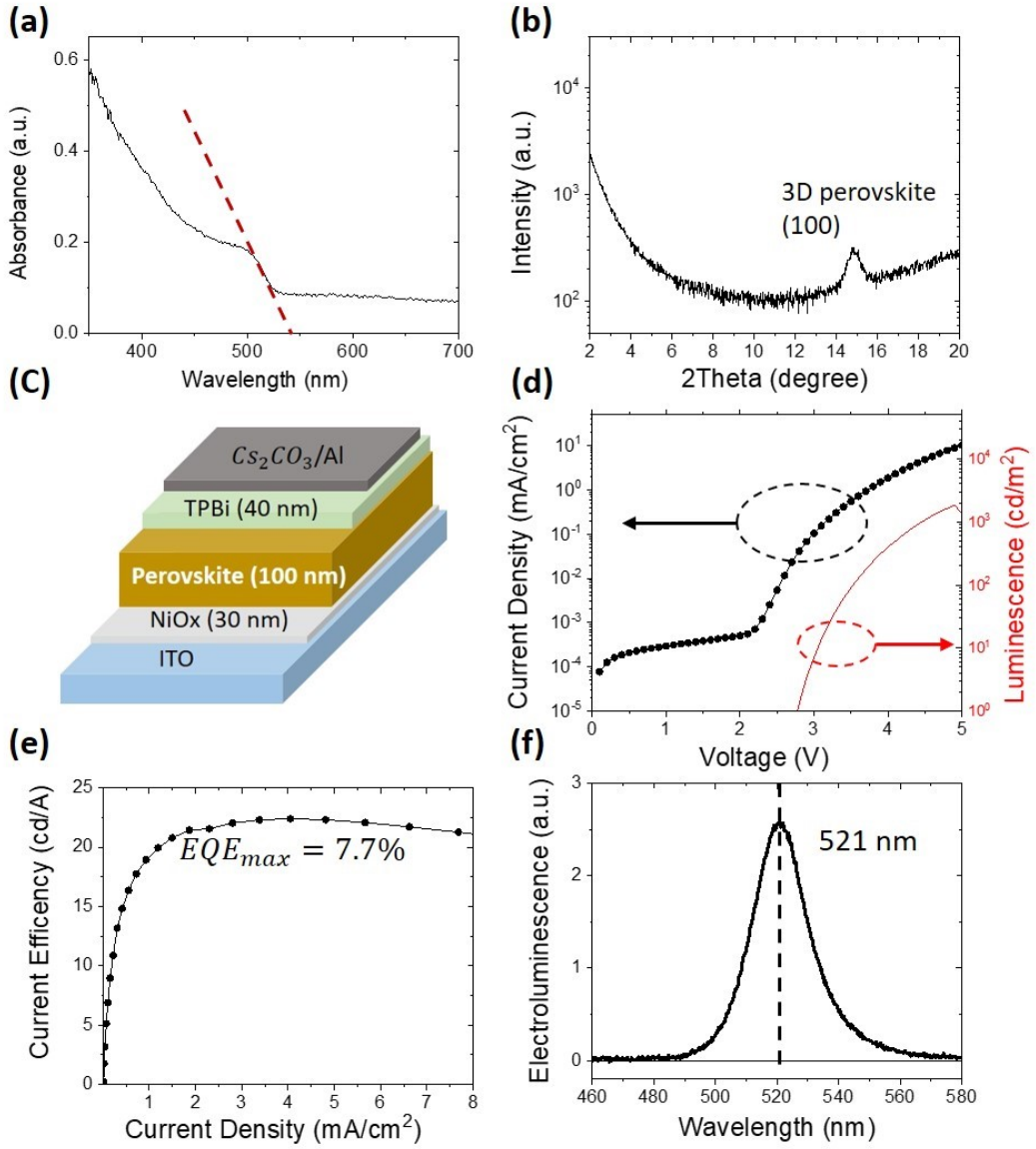


Figure 1. (a) Absorption and (b) X-ray diffraction of the perovskite film. (c) Schematic diagram of the device structure. (d) JVL curve and (e) current efficiency of the perovskite LED. (f) Spectrum of electroluminescence at 3.8 V.

### 2.2. Transient Behaviors of Perovskite LED

To study the device operation mechanism and the effects of ion migration on device performance, Tr-EL and Tr-J measurements were conducted by applying a pulse voltage (pulse width is 50 ms; frequency is 4 Hz; reference voltage is 0 V) on the device and monitoring the transient EL intensity

and current density by an oscilloscope, and the results are shown in Figures 2 (a) and (b). From the results of the Tr-EL measurements, we found that the EL response time is up to 20 ms, which is almost four orders of magnitude longer than that in typical OLEDs.[32,33] It should be noted that the EL response time in OLEDs is mostly limited due to the carrier transit time in the devices which is typically on the order of a few microseconds depending of the carrier mobilities of the electron and hole transporting layers. From the results of Tr-J measurements, we observed a sharp peak in the beginning, followed by a slow increase also in a time scale of tens of milliseconds. The initial sharp rise comes from the RC response (estimated to be 0.125 ms) of the equivalent circuit of the device,[34] which is much longer than that in typical OLEDs.[33] We attribute this large RC response to ion migration in the perovskite resulting from the capacitance contribution due to ionic polarization.[25] The subsequent slow increase of the current partially accounts for the slow EL response. In order to determine whether the slow increase of the current is the only reason for the slow EL response, we divided the EL by the current density to extract the transient current efficiency of the device (Figure 2 (c)). From the results, the efficiency also shows a slow response in a similar time scale. Therefore, the slow EL response is a combined result of the slow current response and the slow efficiency response. Since the transient current is an indication of the charge injection dynamics and the transient efficiency is an indication of the charge recombination dynamics, to better understand the operation mechanism of the perovskite LED, we carried out in-depth studies on these two aspects in the following sections.

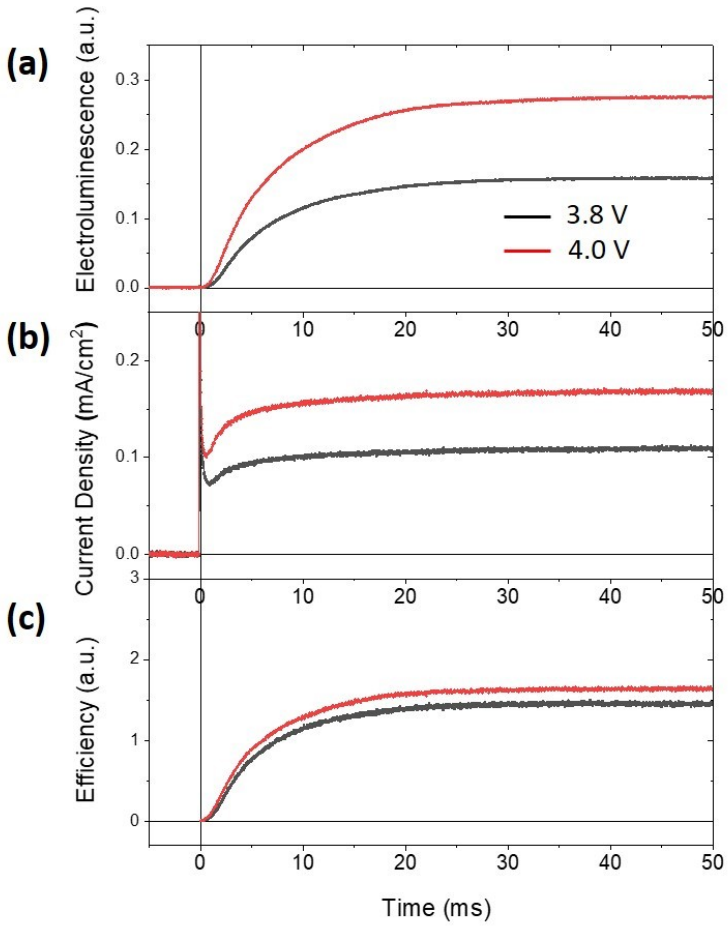


Figure 2. Transient (a) electroluminescence and (b) current (c) efficiency of the perovskite LED at different pulse voltages (pulse width=50 ms, frequency=4 Hz, reference voltage=0 V).

### 2.3. Charge Injection Dynamics

The slow current response (Figure 2 (b)) of our perovskite LED can be attributed to ion migration in the perovskite. It has been reported that mobile ions in perovskites under electric field can migrate to the electrode interface.[25–27] When applying a forward bias to a perovskite LED, negative halide ions migrate to the anode interface facilitating hole injection, while positive $MA^+$ migrate to the cathode interface facilitating electron injection. Compared with the transport of charge carriers, the migration of ions is much slower, typically in a time scale of millisecond to second.[24] Therefore, the enhancement of charge injection facilitated by ion migration is expected to be slow,

leading to a slow increase in the current. However, the slow current response of the perovskite LED is a combined result of electron and hole injection dynamics. To have a detailed understanding of the effect of ion migration on charge injection, we conducted Tr-J measurements on single carrier devices to examine the injection dynamics of electrons and holes separately.

Electron-only and hole-only devices fabricated have the following structures respectively: ITO/ aluminum-doped zinc oxide (AZO)/ perovskite/ TPBi/ $Cs_2CO_3$/ Al and ITO/ $NiO_x$/ perovskite/ $MoO_x$/ Au. In both cases, EL was not observed when current was injected into the devices, indicating they are truly single carrier devices. Tr-J measurements were conducted on single carrier devices by applying a pulse voltage (pulse width is 50 ms, frequency is 4 Hz, reference voltage is 0 V) and monitoring the evolution of the current density with time, and the results are shown in Figure 3. From the hole-only device Tr-J data (Figure 3 (a)), after the initial RC response, there is a slow increase in the hole current with a time scale on the order of tens of milliseconds, similar to that of the current response of the perovskite LED. Therefore, we conclude that hole injection is enhanced by the accumulation of Br ions at the anode interface, contributing to the slow current response of the perovskite LED. From the electron-only device Tr-J data (Figure 3 (b)), we observed a decrease after the initial RC response, indicating it does not contribute to the slow current response of the perovskite LED. The decrease of the electron current can be attributed to a screening effect of ionic polarization on the external electric field (the pulse voltage):[34] ion-migration-induced polarization generates an internal electric field which is in the opposite direction of the external electric field, leading to a decrease in the total electric field in the perovskite layer, thereby impeding the charge transport. In principle, hole transport in perovskite should also be affected by this screening effect. However, the enhanced hole injection at the anode interface due to ion migration plays a dominant role so that we mainly observed the slow increase

in hole current.

The very different electron and hole injection dynamics indicate that Br ions are the primary species responsible for ion migration in the perovskite layer. Our results appear to be different from those previously show that A-site cations ($MA^+$) are responsible for ion migration.[35,36] Such a discrepancy originates from two reasons. First, most previous works on ion migration use bulk 3D perovskites where the grain boundaries are the main channel of migration for both $MA^+$ and halide ions,[36–38] while in our case, the grain boundaries are passivated by the bulky organic cations, leaving the grain interior being the main channel.[39,40] Without the grain boundaries, migration of $MA^+$ is largely suppressed such that we did not observe migration of the A-site cations, and halide ions are still mobile inside the grain due to their much lower activation energy compared with $MA^+$.[41,42] From this point of view, the migration of Br ions in our perovskites is confined within the $MAPbBr_3$ nanocrystals, and the enhanced hole injection is due to the migration of the mobile Br ions in the $MAPbBr_3$ nanocrystals adjacent to the HTL interface. Second, the timescale we used for the measurements is different from previous works. For example, in a previous work reported the migration of $MA^+$ in quasi-2D perovskites, the authors studied the device degradation mechanism in a timescale of hundreds of second,[43] while in our case, we study the device operation mechanism in a timescale of tens of millisecond. In the long timescale (above 100 s) measurements, the migration of $MA^+$ can be observed due to the continuous electric stress leading to decomposition of the perovskite,[43,44] while in our short timescale (within 100 millisecond) measurements, only halide ion migration is detected due to the short pulse duration that does not lead to structural decomposition. This is supported by our observation that the shape of the transient curves on the oscilloscope does not change during the repeated measurements, indicating that Br ions return to their original positions after the voltage is removed. Therefore, our results

bring new insights to the understanding of ion migration in perovskite LEDs.

From Figure 3, it is noted that the steady-state hole current is more than an order of magnitude larger than the steady-state electron current, indicating a strong charge imbalance of the resulting perovskite LED during steady-state operation. This strong charge imbalance can be attributed to Br ion migration: due to the existence of the bulky organic cations, charge injection into the perovskite layer is supposed to be impeded; however, the injection of holes is facilitated by Br ion migration while the injection of electrons is suppressed by the ionic-polarization-induced screening effect as discussed previously, leading to a much larger steady-state hole current than the electron current. This explanation is also consistent with the observation that the increase in hole current becomes smaller at a lower voltage (2.0 V), since the increase relies on the external electric field driving the Br ions to the HTL interface. More importantly, the strong charge imbalance induced by ion migration leads to a narrow recombination zone located at the ETL interface thereby limits the device efficiency. The implication of this important finding is that electron injection is the bottleneck to the device performance. Finally, it should be noted that the origin of the charge imbalance cannot be revealed by steady-state measurements, and temperature-dependent transient current measurements are needed to understand the device operation mechanism.

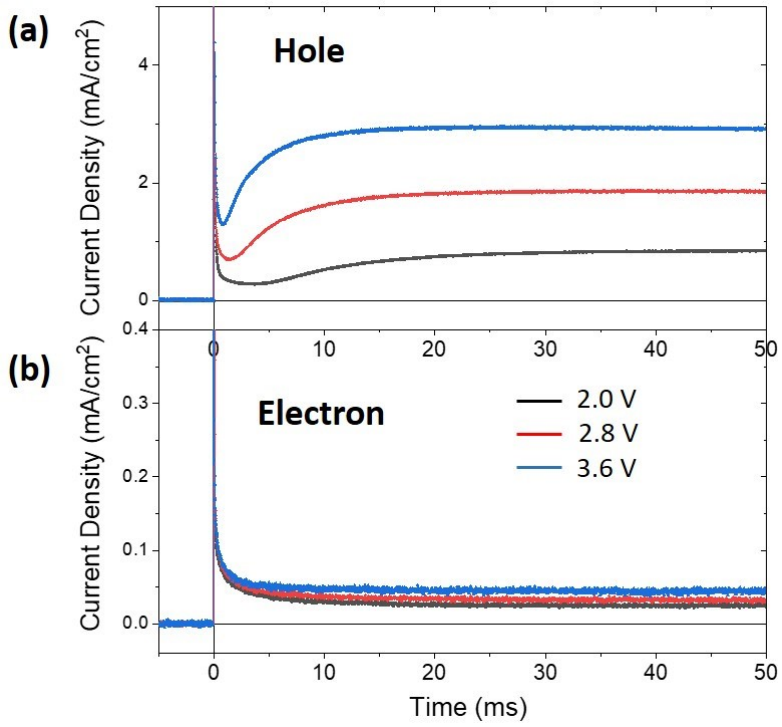


Figure 3. Transient current of (a) the hole-only device and (b) the electron-only device under different pulse voltages (reference voltage=0, frequency=4 Hz, pulse width=50 ms).

Here, we conducted temperature-dependent Tr-J measurements on hole-only devices to extract the activation energy of Br ion migration and the results are shown in Figure 4. As expected, we observed slower responses of hole current at lower temperatures. In addition, at lower temperatures, there is a decrease of the initial RC response prior the slow increase. As mentioned previously, this decrease is attributed to the screening effect of ionic polarization resulted in reduction of the electric field in the perovskite layer.[34] Therefore, to quantify the hole current, we divide it into three components with each one expressed by an exponential term:[34] (i) the initial RC response, $A_1\exp(-t/\tau_1)$; (ii) the decrease of the hole current due to the screening effect induced by Br ion migration, $A_2\exp(-t/\tau_2)$; (iii) the increase of the hole current due to the enhanced hole injection facilitated by the accumulation of Br ions at the anode interface, $A_3\exp(-t/\tau_3)$. Therefore, the hole

current can be expressed using the equation below:

$$J = A_1 \exp\left(-\frac{t}{\tau_1}\right) + A_2 \exp\left(-\frac{t}{\tau_2}\right) + A_3 \exp\left(-\frac{t}{\tau_3}\right) + A_0 \qquad (1)$$

We fitted the measured hole current with Equation (1) and the results are shown in Figure 4. Fitting parameters are summarized in Table S1. Here, $\tau_2$ and $\tau_3$ are both due to Br ion migration, thus indicating the characteristic time of Br ion migration in the perovskite. Therefore, we have the following approximate relationships:[34]

$$k_2 = \frac{1}{\tau_2} \sim \sigma = C \exp\left(-\frac{E_a}{kT}\right) \qquad (2) \qquad k_3 = \frac{1}{\tau_3} \sim \sigma = C \exp\left(-\frac{E_a}{kT}\right) \qquad (3)$$

where σ is the ionic conductivity, C is a constant coefficient, $E_a$ is the activation energy of Br ion migration, k is the Boltzmann constant and T is the temperature. To extract the activation energy, we conducted linear fittings on ln ($k_2$) and ln ($k_3$) versus 1/kT, and the results are shown in Figure 5. The slopes of the linear fittings give the activation energy. From the results, we found that the activation energy extracted from $k_2$ (0.20 eV) is close to that of $k_3$ (0.18 eV), which is about the same as expected since they are both induced by Br ion migration. Therefore, the activation energy of Br ion migration in our perovskite is calculated to be 0.18~0.20 eV, consistent with the values reported in the literature.[45–47] This quantitative analysis verifies that the slow hole current response is induced by Br ion migration.

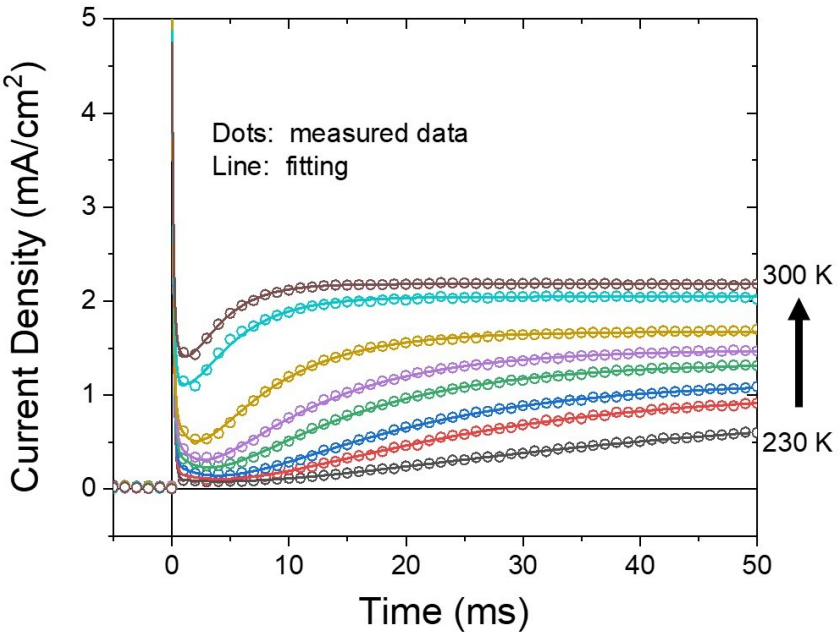


Figure 4. Transient current of the hole-only device at different temperatures with pulse voltage being 3.0 V (reference voltage=0 V, frequency=4 Hz, pulse width=50 ms). The temperature increment is 10 K. Hollow dots are experimental data, while solid lines are fitted curves.

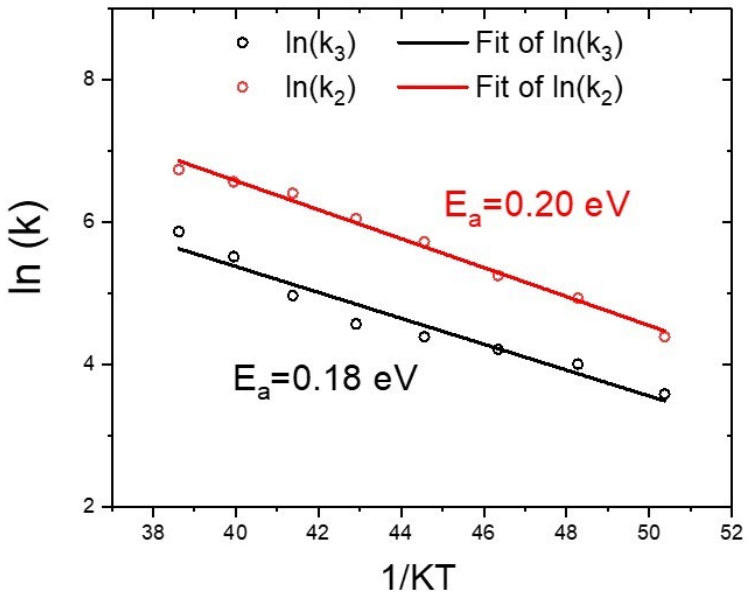


Figure 5. Extract activation energy of Br ion migration by linear fitting.

### 2.4. Charge Recombination Dynamics

In addition to the charge injection dynamics as we addressed in the last section, charge recombination dynamics is another fundamental process in the operation of a perovskite LED, resulting in a slow efficiency response (Figure 2 (c)). One of the reasons for the slow efficiency response is the enhanced charge injection facilitated by ion migration increasing the carrier density in the perovskite layer. Since defect-assisted non-radiative recombination is monomolecular and radiative recombination is bimolecular, we expect that a higher carrier density in the perovskite layer favors radiative recombination.[21] Under forward bias, hole injection in the perovskite LED is enhanced, leading to an accumulation of excess holes at the ETL/perovskites interface, which subsequently facilitates electron injection into the perovskite layer. Therefore, the increased injected carrier density in the perovskite layer results in an enhanced efficiency, leading to a slow increase in efficiency. Further, a reduction of defect density in perovskite under electric field could

be another reason for the higher efficiency. It has been reported that under photoexcitation or electric field, pairs of halide interstitials and vacancies migrate and annihilate in perovskite, leading to a reduction of defect density and an increase in radiative recombination efficiency.[29–31] To determine whether this effect also contributes to the slow response of the efficiency, we conducted PL measurements under pulse voltage to investigate the effects of electric field on radiative recombination.

In order to rule out EL and the effects of charge injection on PL, the device used for the PL measurements has a structure of ITO/ $HfO_2$ (40 nm)/ perovskite/ Poly (methyl methacrylate) (PMMA) (40 nm)/Al, where $HfO_2$ and PMMA are two insulating layers blocking charge injection. The experimental set-up is shown in Figure 6 (a): the perovskite sample is excited by a 405 nm diode laser under an applied pulse voltage and the PL intensity is monitored by a photodetector with the signal connected to an oscilloscope. The measurement results are shown in Figure 6 (b). From the results, we found that the applied electric field has a small effect on the PL intensity, indicating that the radiative recombination efficiency is only slightly perturbed by the electric field. To understand the origin of this perturbation, we magnified the signals and the data are shown in Figure 6 (c). Here, the PL data shows five characteristic regions: region 1 is a constant PL intensity without external electric field; region 2 is an abrupt drop of the PL intensity right after the application of the external electric field (pulse voltage); region 3 is a slow increase in the PL intensity under the external electric field; region 4 is an abrupt drop of the PL intensity right after the removal of the external electric field; region 5 is a slow recovering of PL after the removal of the external electric field.

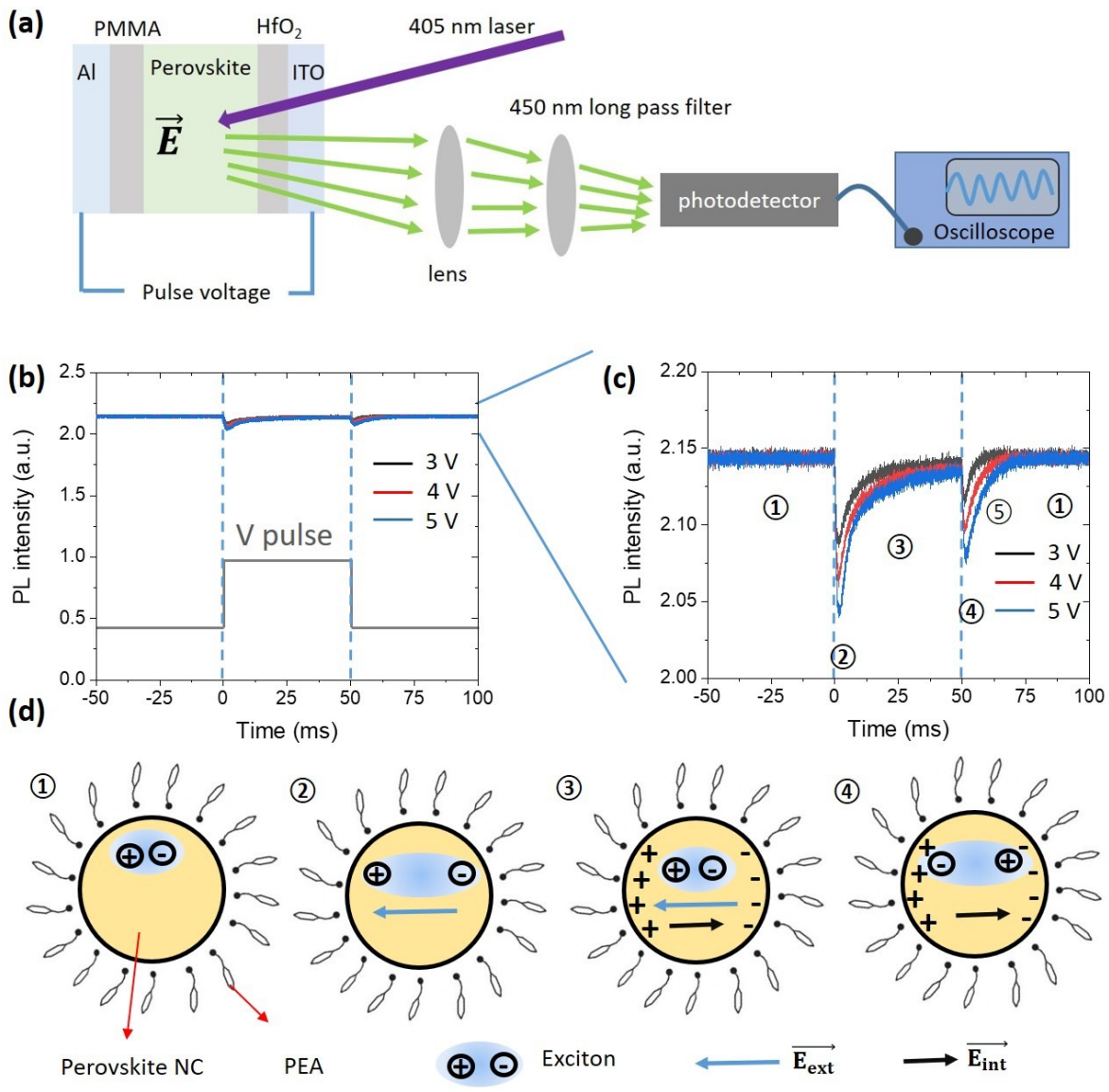


Figure 6. (a) Schematic diagram showing the set-up of PL under pulse voltage. (b) Photoluminescence (PL) of a perovskite device (ITO/$HfO_2$/perovskite/PMMA/Al) under different pulse voltages. (c) Magnification of (b). (d) Schematic diagrams illustrating the effects of electric field on exciton dynamics at different regions of (b): ① no electric field; ② external electric field separates exciton; ③ external electric field is screened by internal electric field induced by ion migration; ④ ion-migration-induced internal electric field separates exciton.

We propose that the evolution of the PL intensity can be explained by Br ion migration in the perovskite layer. As we mentioned previously, we have perovskite nanocrystals ($MAPbBr_3$) embedded in an organic matrix (PEABr), as shown in Figure 6 (d) ①. Therefore, both excitons

and mobile ions are confined in the nanocrystals. From region 1 to region 2, upon an application of the electric field, electrons and holes are pulled away from each other in the nanocrystals, leading to an abrupt decrease in the radiative recombination efficiency[48] (Figure 6 (d) ①&②). From region 2 to region 3, ion-migration-induced polarization driven by the external electric field generates an internal electric field that is in the opposite direction. As a result, the total electric field is decreased, leading to a slow increase in the radiative recombination efficiency (Figure 6 (d) ②&③). From region 3 to region 4, the external electric field is instantly removed, leaving the internal electric field alone in the perovskite. Therefore, the total electric field is abruptly reversed and increased, leading to an abrupt decrease in the radiative recombination efficiency (Figure 6 (d) ③&④). From region 4 to region 5, without external electric field, mobile halide ions diffuse back, leading to a decrease in the total electric field and a recovery of the radiative recombination efficiency.

Based on the analysis above, we conclude that the small perturbation (about 10%) on PL by the voltage pulse is due to the interplay between the applied external electric field and the ion-migration-induced internal electric field. Here, we do not observe any evidence of the reduction of defect density in perovskite under electric field. It should be noted that the change in the PL intensity due to electric field is very small compared with the change in the EL efficiency, indicating that the slow efficiency response of the perovskite LED is mainly due to the enhanced charge injection that increases the carrier density in the perovskite layer.

Combining the investigations on charge injection and recombination dynamics, we present the operation of the device in Figure 7. As soon as a forward bias is applied (Figure 7 (a)), limited charge carriers are injected into the perovskite layer resulting in a low EL intensity. As the

electrical stress continues (Figure 7 (b)), mobile Br ions in the perovskite layer migrate to the HTL/perovskite interface, facilitating hole injection. The increased hole injection efficiency leads to an accumulation of excess holes at the ETL/perovskites interface, which subsequently facilitates electron injection into the perovskite layer, resulting in a slow increase of the current. In addition, due to the enhanced charge injection efficiency, both the density of electron and hole are increased in the perovskite layer, which favors bimolecular radiative recombination, leading to a slow increase of the efficiency. The slow current response and the slow efficiency response together result in the slow EL response.

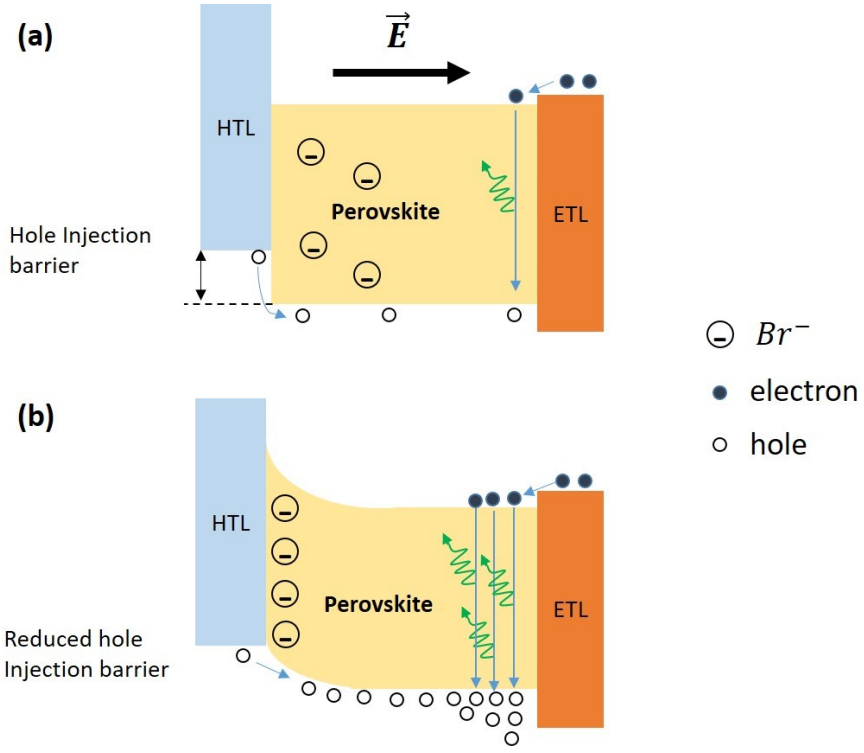


Figure 7. Schematic diagram showing the role of halide ions in the operation of perovskite LED. (a) In the beginning of the pulse voltage. (b) At 10 ms of the pulse voltage.

## 3. Conclusion

In this work, we studied the role of ion migration in the operation of perovskite LEDs by transient

measurements, where the EL intensity, the current density and the device efficiency all show a slow response in a time scale of tens of milliseconds. Through Tr-J measurements on single carrier devices, the data revealed that the slow current response is due to a slow hole injection response which is attributed to the migration and accumulation of the Br ions at the anode interface facilitating hole injection. On the contrary, electron injection is not affected by ion migration. Such a different effect of ion migration on electron and hole injection leads to a strong charge imbalance, suggesting that to enhance the device efficiency electron injection needs to be significantly enhanced to compensate for the enhanced hole injection facilitated by halide ion migration. In addition, through PL measurements under pulse voltage, we identified that the slow efficiency response is mainly attributed to the enhanced charge injection which leads to an increased carrier density favoring bimolecular radiative recombination. Our findings shed light on the understanding of the device physics of perovskite LEDs, thereby paved the way for the future design of device architecture and materials to realize the full potential of perovskites LEDs.

## 4. Experimental Details

### 4.1. Materials

Nickel acetate tetrahydrate (99.998% trace metal basis), ethanol (99.5%, anhydrous), ethanolamine (99.0% ACS reagent), lead bromide (99.999% trace metals basis), N,N-dimethylformamide (DMF) (99.8%, anhydrous), dimethyl sulfoxide (DMSO) (99.9%, anhydrous), chlorobenzene (CB) (99.8%, anhydrous) cesium carbonate ($Cs_2CO_3$) (99.9%, trace metal basis), polyvinylpyrrolidone (PVP), Aluminum-doped zinc oxide (AZO) (2.5 wt %) nanoparticle ink and Poly(methyl methacrylate) (PMMA) are from Sigma Aldrich. Phenethylammonium bromide (PEABr) and methylammonium bromide (MABr) are from Dyesol. 2,2′,2"-(1,3,5-Benzinetriyl)-tris(1-phenyl-1-H-benzimidazole) (TPBi) is from Lumtec. Aluminum pellets, Gold pellets and $MoO_x$ are from

Kurt J. Lesker.

**4.2. Device Fabrications**

For the perovskite LEDs, glass substrates with ITO pattern were cleaned by acetone and isopropanol in sequence in ultrasonic bath, followed by UV ozone treatment for 15 min before using. Nickel oxide thin films were fabricated by sol-gel method: 248.8 mg of nickel acetate tetrahydrate and 60 uL of ethanolamine were dissolved into 5 mL of ethanol, which was stirred at 65 ℃ for 45 min to form a stable sol-gel. Then the nickel oxide precursor was spin coated on the cleaned substrates at a speed of 3000 rpm for 1 min, followed by annealing in ambient at 500 ℃ for 1 hour. Perovskite films were fabricated on the nickel oxide film by spin coating method assisted with anti-solvent treatment in nitrogen-filled glove box. The precursor solution of the perovskite was prepared by dissolving 108 mg of lead bromide, 33 mg of MABr and 17.8 mg of PEABr into 1 mL of a mixed solvent (DMSO/DMF=12/88). Before fabricating perovskite films, a solution of PVP (4 mg/mL in DMF) was spin coated on the nickel oxide film at a speed of 4000 rpm to passivate the surface defects of the nickel oxide, followed by annealing at 120 ℃ for 10 min. Then the perovskite solution was spin coated on the passivated nickel oxide film at a speed of 4000 rpm for 2 min, during which 100 uL of CB was dropped on the sample at $5^{th}$ second. After spin coating, the sample was annealed at 80 ℃ for 10 min to evaporate the residual solvents and complete the crystallization of perovskite. To complete the device, 40 nm of TPBi as electron transporting layer and $Cs_2CO_3$ (2nm)/Al (100nm) as cathode were thermally evaporated in sequence on the perovskite film. For the electron-only devices, the $NiO_x$ layer was replaced by AZO layer which was fabricated by spin coating AZO nanoparticle ink at a speed of 3000 rpm, followed by thermal annealing at 150 degree for 10 min in ambient. For the hole-only devices, TPBi and cathode were replaced by 15 nm of $MoO_x$ and 80 nm of Au, which were thermally

evaporated on the as-prepared perovskite films. For the device that is used for the PL measurement under pulse voltage, 40 nm of $HfO_2$ was fabricated by atomic layer deposition (Ultratech/Cambridge Nanotech Savannah) on cleaned ITO substrate. Then perovskite film was fabricated on the $HfO_2$ layer, followed by spin coating 40 nm of PMMA (20 mg/mL in CB) on the top of the perovskite. Lastly, 100 nm of Al was evaporated on the PMMA layer to complete the device fabrication.

### 4.3. Characterizations

Current-voltage-luminance (J-V-L) measurements were conducted by Keithley 2400 and a photodetector. Electroluminescence spectrum was measured by a high-resolution spectrometer (HR4000) from Ocean Optics. In the transient measurements, a pulse voltage generated by a function generator (Agilent 33220A) was applied to the device. To monitor the dynamics of the electroluminescence in the transient measurements, a photomultiplier tube (PMT) powered by a voltage source (C9525-02 from Hamamatsu) was used, whose signal is connected to an oscilloscope (Tektronix MDO3014). In addition, the device is connected in series with a resistor (9850 ohm) whose voltage signal was led into the oscilloscope to monitor the dynamics of current density. X-ray diffraction was conducted by Rigaku SmartLab X-Ray Diffractometer (XRD). UV-visible absorption was done by Lambda 750 UV/Vis spectrometer from PerkinElmer.

### Acknowledgements

The authors thank the support from National Science Foundation (NSF). In addition, XRD in this work was performed at the Analytical Instrumentation Facility (AIF) at North Carolina State University, which is supported by the State of North Carolina and the National Science Foundation (award number ECCS-1542015). The AIF is a member of the North Carolina Research Triangle Nanotechnology Network (RTNN), a site in the National Nanotechnology Coordinated

Infrastructure (NNCI).

**Supporting Information**. Fitting parameters of hole injection current at different temperatures.

## References

(1) Huang, F.; Li, M.; Siffalovic, P.; Cao, G.; Tian, J. From Scalable Solution Fabrication of Perovskite Films towards Commercialization of Solar Cells. *Energy Environ. Sci.* **2019**, *12*, 518–549.

(2) Liu, X.; Yu, D.; Song, X.; Zeng, H. Metal Halide Perovskites: Synthesis, Ion Migration, and Application in Field-Effect Transistors. *Small* **2018**, *14*, 1801460.

(3) Veldhuis, S. A.; Boix, P. P.; Yantara, N.; Li, M.; Sum, T. C.; Mathews, N.; Mhaisalkar, S. G. Perovskite Materials for Light-Emitting Diodes and Lasers. *Adv. Mater.* **2016**, *28*, 6804–6834.

(4) Shan, Q.; Song, J.; Zou, Y.; Li, J.; Xu, L.; Xue, J.; Dong, Y.; Han, B.; Chen, J.; Zeng, H. High Performance Metal Halide Perovskite Light-Emitting Diode: From Material Design to Device Optimization. *Small* **2017**, *13*, 1701770.

(5) Stylianakis, M. M.; Maksudov, T.; Panagiotopoulos, A.; Kakavelakis, G.; Petridis, K. Inorganic and Hybrid Perovskite Based Laser Devices: A Review. *Materials (Basel).* **2019**, *16*, 859.

(6) Yin, W. J.; Shi, T.; Yan, Y. Unusual Defect Physics in CH3NH3PbI3 Perovskite Solar Cell Absorber. *Appl. Phys. Lett.* **2014**, *104*, 063903.

(7) Buin, A.; Pietsch, P.; Xu, J.; Voznyy, O.; Ip, A. H.; Comin, R.; Sargent, E. H. Materials Processing Routes to Trap-Free Halide Perovskites. *Nano Lett.* **2014**, *14*, 6281–6286.

(8) Steirer, K. X.; Schulz, P.; Teeter, G.; Stevanovic, V.; Yang, M.; Zhu, K.; Berry, J. J. Defect Tolerance in Methylammonium Lead Triiodide Perovskite. *ACS Energy Lett.* **2016**, *1*, 360–366.

(9) Meggiolaro, D.; Motti, S. G.; Mosconi, E.; Barker, A. J.; Ball, J.; Andrea Riccardo Perini, C.; Deschler, F.; Petrozza, A.; De Angelis, F. Iodine Chemistry Determines the Defect Tolerance of Lead-Halide Perovskites. *Energy Environ. Sci.* **2018**, *11*, 702–713.

(10) Alcocer, M. J. P.; Leijtens, T.; Herz, L. M.; Petrozza, A.; Snaith, H. J. Electron-Hole Diffusion Lengths Exceeding Trihalide Perovskite Absorber. *Science (80-. ).* **2013**, *342*, 341–344.

(11) Si, J.; Liu, Y.; He, Z.; Du, H.; Du, K.; Chen, D.; Li, J.; Xu, M.; Tian, H.; He, H.; Di, D.; Lin, C.; Cheng, Y.; Wang, J.; Jin, Y. Efficient and High-Color-Purity Light-Emitting Diodes Based on in Situ Grown Films of CsPbX3 (X = Br, I) Nanoplates with Controlled

Thicknesses. *ACS Nano* **2017**, *11*, 11100–11107.

(12) McMeekin, D. P.; Sadoughi, G.; Rehman, W.; Eperon, G. E.; Saliba, M.; Hörantner, M. T.; Haghighirad, A.; Sakai, N.; Korte, L.; Rech, B.; Johnston, M. B.; Herz, L. M.; Snaith, H. J. A Mixed-Cation Lead Mixed-Halide Perovskite Absorber for Tandem Solar Cells. *Science (80-. ).* **2016**, *351*, 151–155.

(13) Pathak, S.; Sakai, N.; Wisnivesky Rocca Rivarola, F.; Stranks, S. D.; Liu, J.; Eperon, G. E.; Ducati, C.; Wojciechowski, K.; Griffiths, J. T.; Haghighirad, A. A.; Pellaroque, A.; Friend, R. H.; Snaith, H. J. Perovskite Crystals for Tunable White Light Emission. *Chem. Mater.* **2015**, *27*, 8066–8075.

(14) Cao, Y.; Wang, N.; Tian, H.; Guo, J.; Wei, Y.; Chen, H.; Miao, Y.; Zou, W.; Pan, K.; He, Y.; Cao, H.; Ke, Y.; Xu, M.; Wang, Y.; Yang, M.; Du, K.; Fu, Z.; Kong, D.; Dai, D.; Jin, Y.; Li, G.; Li, H.; Peng, Q.; Wang, J.; Huang, W. Perovskite Light-Emitting Diodes Based on Spontaneously Formed Submicrometre-Scale Structures. *Nature* **2018**, *562*, 249–253.

(15) Zhao, B.; Bai, S.; Kim, V.; Lamboll, R.; Shivanna, R.; Auras, F.; Richter, J. M.; Yang, L.; Dai, L.; Alsari, M.; She, X. J.; Liang, L.; Zhang, J.; Lilliu, S.; Gao, P.; Snaith, H. J.; Wang, J.; Greenham, N. C.; Friend, R. H.; Di, D. High-Efficiency Perovskite–Polymer Bulk Heterostructure Light-Emitting Diodes. *Nat. Photonics* **2018**, *12*, 783–789.

(16) Lin, K.; Xing, J.; Quan, L. N.; de Arquer, F. P. G.; Gong, X.; Lu, J.; Xie, L.; Zhao, W.; Zhang, D.; Yan, C.; Li, W.; Liu, X.; Lu, Y.; Kirman, J.; Sargent, E. H.; Xiong, Q.; Wei, Z. Perovskite Light-Emitting Diodes with External Quantum Efficiency Exceeding 20 per Cent. *Nature* **2018**, *562*, 245–248.

(17) Yuan, M.; Quan, L. N.; Comin, R.; Walters, G.; Sabatini, R.; Voznyy, O.; Hoogland, S.; Zhao, Y.; Beauregard, E. M.; Kanjanaboos, P.; Lu, Z.; Kim, D. H.; Sargent, E. H. Perovskite Energy Funnels for Efficient Light-Emitting Diodes. *Nat. Nanotechnol.* **2016**, *11*, 872–877.

(18) Yang, X.; Zhang, X.; Deng, J.; Chu, Z.; Jiang, Q.; Meng, J.; Wang, P.; Zhang, L.; Yin, Z.; You, J. Efficient Green Light-Emitting Diodes Based on Quasi-Two-Dimensional Composition and Phase Engineered Perovskite with Surface Passivation. *Nat. Commun.* **2018**, *9*, 570.

(19) Wang, N.; Cheng, L.; Ge, R.; Zhang, S.; Miao, Y.; Zou, W.; Yi, C.; Sun, Y.; Cao, Y.; Yang, R.; Wei, Y.; Guo, Q.; Ke, Y.; Yu, M.; Jin, Y.; Liu, Y.; Ding, Q.; Di, D.; Yang, L.; Xing, G.; Tian, H.; Jin, C.; Gao, F.; Friend, R. H.; Wang, J.; Huang, W. Perovskite Light-Emitting Diodes Based on Solution-Processed Self-Organized Multiple Quantum Wells. *Nat. Photonics* **2016**, *10*, 699–704.

(20) Xiao, Z.; Kerner, R. A.; Zhao, L.; Tran, N. L.; Lee, K. M.; Koh, T.-W.; Scholes, G. D.; Rand, B. P. Efficient Perovskite Light-Emitting Diodes Featuring Nanometre-Sized Crystallites. *Nat. Photonics* **2017**, *11*, 108–115.

(21) Xing, G.; Wu, B.; Wu, X.; Li, M.; Du, B.; Wei, Q.; Guo, J.; Yeow, E. K. L. L.; Sum, T. C.; Huang, W. Transcending the Slow Bimolecular Recombination in Lead-Halide Perovskites

for Electroluminescence. *Nat. Commun.* **2017**, *8*, 14558.

(22) Chen, B.; Yang, M.; Zheng, X.; Wu, C.; Li, W.; Yan, Y.; Bisquert, J.; Garcia-Belmonte, G.; Zhu, K.; Priya, S. Impact of Capacitive Effect and Ion Migration on the Hysteretic Behavior of Perovskite Solar Cells. *J. Phys. Chem. Lett.* **2015**, *6*, 4693–4700.

(23) Calado, P.; Telford, A. M.; Bryant, D.; Li, X.; Nelson, J.; O'Regan, B. C.; Barnes, P. R. F. Evidence for Ion Migration in Hybrid Perovskite Solar Cells with Minimal Hysteresis. *Nat. Commun.* **2016**, *7*, 13831.

(24) Yuan, Y.; Huang, J. Ion Migration in Organometal Trihalide Perovskite and Its Impact on Photovoltaic Efficiency and Stability. *Acc. Chem. Res.* **2016**, *49*, 286–293.

(25) Zhang, H.; Lin, H.; Liang, C.; Liu, H.; Liang, J.; Zhao, Y.; Zhang, W.; Sun, M.; Xiao, W.; Li, H.; Polizzi, S.; Li, D.; Zhang, F.; He, Z.; Choy, W. C. H. Organic-Inorganic Perovskite Light-Emitting Electrochemical Cells with a Large Capacitance. *Adv. Funct. Mater.* **2015**, *25*, 7226–7232.

(26) Andričević, P.; Mettan, X.; Kollár, M.; Náfrádi, B.; Sienkiewicz, A.; Garma, T.; Rossi, L.; Forró, L.; Horváth, E. Light-Emitting Electrochemical Cells of Single Crystal Hybrid Halide Perovskite with Vertically Aligned Carbon Nanotubes Contacts. *ACS Photonics* **2019**, *6*, 967–975.

(27) Bandiello, E.; Ávila, J.; Gil-Escrig, L.; Tekelenburg, E.; Sessolo, M.; Bolink, H. J. Influence of Mobile Ions on the Electroluminescence Characteristics of Methylammonium Lead Iodide Perovskite Diodes. *J. Mater. Chem. A* **2016**, *4*, 18614–18620.

(28) Kim, H.; Zhao, L.; Price, J. S.; Grede, A. J.; Roh, K.; Brigeman, A. N.; Lopez, M.; Rand, B. P.; Giebink, N. C. Hybrid Perovskite Light Emitting Diodes under Intense Electrical Excitation. *Nat. Commun.* **2018**, *9*, 4893.

(29) DeQuilettes, D. W.; Zhang, W.; Burlakov, V. M.; Graham, D. J.; Leijtens, T.; Osherov, A.; Bulović, V.; Snaith, H. J.; Ginger, D. S.; Stranks, S. D. Photo-Induced Halide Redistribution in Organic-Inorganic Perovskite Films. *Nat. Commun.* **2016**, *7*, 11683.

(30) Zhao, L.; Gao, J.; Lin, Y. H. L.; Yeh, Y. W.; Lee, K. M.; Yao, N.; Loo, Y. L.; Rand, B. P. Electrical Stress Influences the Efficiency of CH3NH3PbI3 Perovskite Light Emitting Devices. *Adv. Mater.* **2017**, *29*, 1605317.

(31) Mosconi, E.; Meggiolaro, D.; Snaith, H. J.; Stranks, S. D.; De Angelis, F. Light-Induced Annihilation of Frenkel Defects in Organo-Lead Halide Perovskites. *Energy Environ. Sci.* **2016**, *9*, 3180–3187.

(32) Lin, M. Te; Li, M.; Chen, W. H.; Omary, M. A.; Shepherd, N. D. Transient Electroluminescence Determination of Carrier Mobility and Charge Trapping Effects in Heavily Doped Phosphorescent Organic Light-Emitting Diodes. *Solid. State. Electron.* **2011**, *56*, 196–200.

(33) Lee, J. H.; Chen, C. H.; Lin, B. Y.; Shih, Y. C.; Lin, K. F.; Wang, L.; Chiu, T. L.; Lin, C. F. Effect of Trapped Electrons on the Transient Current Density and Luminance of Organic Light-Emitting Diode. *J. Phys. D. Appl. Phys.* **2018**, *51*, 144003.

(34) Li, D.; Wu, H.; Cheng, H. C.; Wang, G.; Huang, Y.; Duan, X. Electronic and Ionic Transport Dynamics in Organolead Halide Perovskites. *ACS Nano* **2016**, *10*, 6933–6941.

(35) Yuan, Y.; Chae, J.; Shao, Y.; Wang, Q.; Xiao, Z.; Centrone, A.; Huang, J. Photovoltaic Switching Mechanism in Lateral Structure Hybrid Perovskite Solar Cells. *Adv. Energy Mater.* **2015**, *5*, 1–7.

(36) Yun, J. S.; Seidel, J.; Kim, J.; Soufiani, A. M.; Huang, S.; Lau, J.; Jeon, N. J.; Seok, S. Il; Green, M. A.; Ho-Baillie, A. Critical Role of Grain Boundaries for Ion Migration in Formamidinium and Methylammonium Lead Halide Perovskite Solar Cells. *Adv. Energy Mater.* **2016**, *6*, 1–8.

(37) Meggiolaro, D.; Mosconi, E.; De Angelis, F. Formation of Surface Defects Dominates Ion Migration in Lead-Halide Perovskites. *ACS Energy Lett.* **2019**, *4*, 779–785.

(38) Shao, Y.; Fang, Y.; Li, T.; Wang, Q.; Dong, Q.; Deng, Y.; Yuan, Y.; Wei, H.; Wang, M.; Gruverman, A.; Shield, J.; Huang, J. Grain Boundary Dominated Ion Migration in Polycrystalline Organic-Inorganic Halide Perovskite Films. *Energy Environ. Sci.* **2016**, *9*, 1752–1759.

(39) Xiao, X.; Dai, J.; Fang, Y.; Zhao, J.; Zheng, X.; Tang, S.; Rudd, P. N.; Zeng, X. C.; Huang, J. Suppressed Ion Migration along the In-Plane Direction in Layered Perovskites. *ACS Energy Lett.* **2018**, *3*, 684–688.

(40) Lin, Y.; Bai, Y.; Fang, Y.; Wang, Q.; Deng, Y.; Huang, J. Suppressed Ion Migration in Low-Dimensional Perovskites. *ACS Energy Lett.* **2017**, *2*, 1571–1572.

(41) Azpiroz, J. M.; Mosconi, E.; Bisquert, J.; De Angelis, F. Defect Migration in Methylammonium Lead Iodide and Its Role in Perovskite Solar Cell Operation. *Energy Environ. Sci.* **2015**, *8*, 2118–2127.

(42) Eames, C.; Frost, J. M.; Barnes, P. R. F.; O'Regan, B. C.; Walsh, A.; Islam, M. S. Ionic Transport in Hybrid Lead Iodide Perovskite Solar Cells. *Nat. Commun.* **2015**, *6*, 7497.

(43) Cheng, T.; Tumen-Ulzii, G.; Klotz, D.; Watanabe, S.; Matsushima, T.; Adachi, C. Ion Migration-Induced Degradation and Efficiency Roll-off in Quasi-2D Perovskite Light-Emitting Diodes. *ACS Appl. Mater. Interfaces* **2020**, *12*, 33004–33013.

(44) Prakasam, V.; Tordera, D.; Bolink, H. J.; Gelinck, G. Degradation Mechanisms in Organic Lead Halide Perovskite Light-Emitting Diodes. *Adv. Opt. Mater.* **2019**, *7*, 1–7.

(45) Meloni, S.; Moehl, T.; Tress, W.; Franckeviius, M.; Saliba, M.; Lee, Y. H.; Gao, P.; Nazeeruddin, M. K.; Zakeeruddin, S. M.; Rothlisberger, U.; Graetzel, M. Ionic Polarization-Induced Current-Voltage Hysteresis in CH3NH3PbX3 Perovskite Solar Cells. *Nat.*

*Commun.* **2016**, *7*, 10334.

(46) Chen, M.; Shan, X.; Geske, T.; Li, J.; Yu, Z. Manipulating Ion Migration for Highly Stable Light-Emitting Diodes with Single-Crystalline Organometal Halide Perovskite Microplatelets. *ACS Nano* **2017**, *11*, 6312–6318.

(47) Oranskaia, A.; Yin, J.; Bakr, O. M.; Brédas, J. L.; Mohammed, O. F. Halogen Migration in Hybrid Perovskites: The Organic Cation Matters. *J. Phys. Chem. Lett.* **2018**, *9*, 5474–5480.

(48) Xu, Z.; De Rosia, T.; Weeks, K. Photoluminescence-Voltage (PL-V) Hysteresis of Perovskite Solar Cells. *J. Phys. Chem. C* **2017**, *121*, 24389–24396.

**TOC graph**